Advanced Composite Materials
Publication details, including instructions for authors and subscription information:
http://www.tandfonline.com/loi/tacm20

Experimental Study on Ni-Base Alloy Bulk Reinforced by Laser Sintered WC Particles

Jinsong Chen [a], Yinhui Huang [b], Xuesong Gao [c], Bin Qiao [d], Jianming Yang [e] & Yiqiang He [f]

[a] College of Mechanical Engineering, Huaihai Institute of Technology, Lianyungang 222005, People's Republic of China;, Email: jinsong20001@163.com

[b] College of Mechanical and Engineering, Nanjing University of Aeronautics & Astronautics, Nanjing 210016, People's Republic of China

[c] College of Mechanical and Engineering, Nanjing University of Aeronautics & Astronautics, Nanjing 210016, People's Republic of China

[d] College of Mechanical Engineering, Huaihai Institute of Technology, Lianyungang 222005, People's Republic of China

[e] College of Mechanical Engineering, Huaihai Institute of Technology, Lianyungang 222005, People's Republic of China

[f] College of Mechanical Engineering, Huaihai Institute of Technology, Lianyungang 222005, People's Republic of China

Version of record first published: 02 Apr 2012.

VSP

Advanced Composite Materials 20 (2011) 277–287

ADVANCED COMPOSITE MATERIALS
brill.nl/acm

Experimental Study on Ni-Base Alloy Bulk Reinforced by Laser Sintered WC Particles

Jinsong Chen [a,*], **Yinhui Huang** [b], **Xuesong Gao** [b], **Bin Qiao** [a], **Jianming Yang** [a] **and Yiqiang He** [a]

[a] College of Mechanical Engineering, Huaihai Institute of Technology, Lianyungang 222005, People's Republic of China

[b] College of Mechanical and Engineering, Nanjing University of Aeronautics & Astronautics, Nanjing 210016, People's Republic of China

Received 7 May 2010; accepted 3 November 2010

Abstract

The basic principle of the formation of high-temperature Ni-base alloy reinforced by tungsten (wolfram) carbide (WC) particles using the technique of direct metal laser sintering (DMLS) was introduced. The effect of different process parameters (laser power, scanning rate) on the micro-topography, composition and micro-hardness of the sintered area is studied by means of scanning electron telescope, X-ray diffractometer and micro-hardness tester. At a laser power of 900 W and a scanning rate of 0.7 m/min, the test shows good laser sintering performance and high sintered density. Meanwhile, it indicates that WC particles are molten into dendritic crystals and evenly dispersed in the matrix, and that the reinforced particles are arrested by the solid–liquid interface. The fact that WC particles are well dispersed in the matrix improves the performance of the bulk sintering. According to the test, we have obtained a set of optimal process parameters in production of sintered metal bulks, high in hardness and compact in construction.

Keywords

Laser sintered, Ni-base alloy bulk, scanning rate, laser power, sintering density

1. Introduction

Short in production cycle and high in part formability, DMLS has been gradually used for manufacturing complex molds in small batch [1–3]. Under computer control, the metal parts of complex shape, which are impossible to produce by use of the traditional processes, can be manufactured easily and quickly using DMLS, e.g., the parts which are hollow. Compared with other laser sintering processes, the greatest advantage of DMLS is that the finished metal parts require no after-treatment and

* To whom correspondence should be addressed. E-mail: jinsong20001@163.com
Edited by the JSCM

DOI:10.1163/092430410X547092

display high density after formation. Therefore, DMLS has come to be the most effective process in response to the current problem. As high-temperature nickel-base cast alloy used for high-temperature gas passage needs higher temperature strength and better resistance to oxidization/corrosion, WC–Ni kentanium of great hardness was added in this experiment based on Ni-base alloy powder, where kentanium of high strength and low tenacity precisely complemented the Ni-base alloy powder. Meanwhile, the Ni could wet the WC very effectively [4–6], so it is a good compound powder for use in laser sintering.

Ni-base alloy boasts good high-temperature strength, oxidization and corrosion resistance, fatigue performance and rupture tenacity, etc.; it is stable in structure and reliable in application in different temperatures. As Ni-base alloy plays an extremely important role in the field of high-temperature alloy, it is widely used to manufacture aviation-purposed jet engines and the parts at the ultimately hot end of various industrial gas turbines. On the other hand, however, high-temperature Ni-base alloy is poor in workability due to its own characteristics, especially when used to manufacture the parts of complex shape, so its application is limited.

The phase, organization and other mechanical properties of laser sintered specimen was studied in this paper according to the sintering test over Ni-base alloy powder containing a given quantity of WC–Ni in different laser parameters, in order to determine the action of WC on Ni-base alloy matrix and the optimal sintering parameters.

2. Materials and Experimental Method

The compound ceramic powder is KF-56 WC–Ni 12% (Ni-coated WC) micron compound powder, WC mass fraction 88% and excess Ni, whose microphotograph is shown in Fig. 1. In unsintered primitive compound powder, the particle of Ni-coated WC is an irregular polyhedron, in which the width and length are between 50–80 μm and 90–150 μm, respectively. As Fig. 2 shows, the characteristic diffraction maximum of Ni in a single Ni-coated WC particle is very sharp. It shows that the content of Ni is 92.17 wt%, but W just only 0.98 wt%. It prove that Ni, as binding phase, has almost completely coated the WC particle in a single Ni-coated WC particle.

High-temperature Ni-base alloy is just KGH95 Ni-base alloy powder. We put Ni-base alloy powder at a mass proportion 70:30 and WC–Ni 12% powder in the vacuum ball grinder and mixed them: grinding media to material: 5:1, rotation rate: 200 r/min, and grinding time 50 min.

This experiment employed the SLCF-X12 $\times$ 25 multi-function CO_2 laser machine tool produced by Shanghai Unity Prima Laser Equipment Co. Ltd. to conduct DLMS sintering test, whose maximal output power is 2 kW, with power adjustable continuously. Automatic power coater was used and laser sintering was carried out at room temperature without addition of a protective atmosphere. The parameters

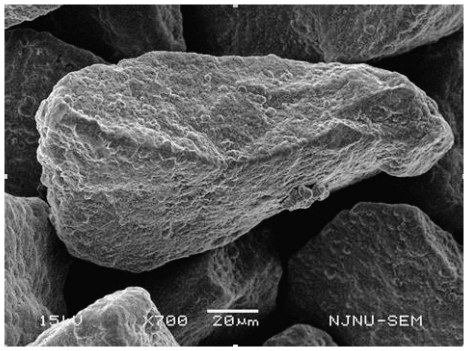

Figure 1. SEM of WC particles.

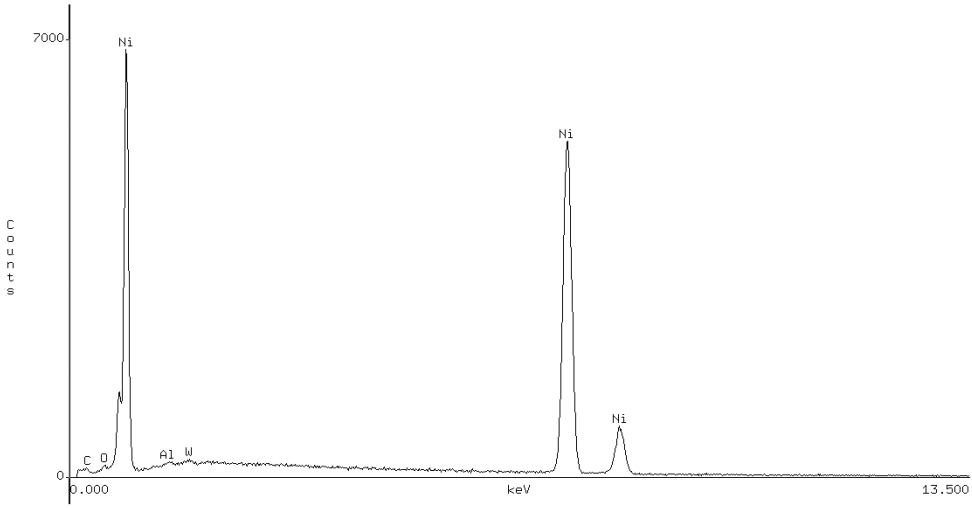

Figure 2. EDS spectrum of a single Ni-coated WC particle.

include spot diameter 1.0 mm, powder coating thickness 1.0 mm, scanning rate 0.4–0.9 m/min, scanning interval 1.0 mm and laser power 500–1000 W.

The density of the laser molded specimen was determined according to the Law of Archimedes. The phase of the sintered specimen was analyzed by means of D/MAXRC XRD; the micro topography of sintered bulks was taken by means of LEO1530VP SEM; the micro-hardness of the specimen was determined at a load of 4.9 N by means of HXS-I000 AK micro hardness tester for 15 s.

3. Laser Molding Process

In the course of laser sintering, the critical factors affecting the sintering quality are the properties and sintering temperature of the powder itself. As the former has been identified, this experiment focused on control of the parameters which affect

sintering temperature. The temperature of powder in sintering can be expressed approximately as follows [7]:

$$T = \frac{2\alpha_A P}{\lambda_t b v}\sqrt{\frac{\alpha_t t}{\pi}}, \tag{1}$$

where t is the time that the laser acts on the material, which may be expressed approximately as the spot diameter divided by the scanning rate; α is the ratio of absorption of laser energy by the surface of the sintered powder; α_t, the ratio of heat diffusion of the material; λ_t, the ratio of heat conduction; P, the power of laser, b, the spot diameter; and v, the scanning rate.

According to equation (1), the sintering temperature of the material surface and the laser power P are directly proportional: where P increases, the sintering temperature rises as well. The sintering temperature and the scanning rate however are inversely proportional: where the sintering temperature of the material surface falls, the scanning rate increases. When the powder is given, the laser power and the scanning rate are the most important factors which affect sintering temperature among the laser sintering parameters. Therefore, this experiment is especially designed to study sintered bulks by regarding laser sintering power and scanning rate as variable parameters.

Figure 3(a) shows the single-line sintering at a scanning rate 0.7 m/min and in different laser powers, where the lines 1–6 are the single-line sintering pattern corresponding to the laser power 500–1000 W, respectively. When the laser power was less than 700 W, lines could not be formed because the laser power was too low and the sintered powder failed to be completely molten. With laser power increasing, the powder became fully molten, thus forming uniform lines. According to the single-line scan, the laser sintering was in the best condition when the laser power reached 900 W. Therefore, this test selected the sintering parameters of lines 4, 5 and 6 in the figure for bulk sintering.

Figure 3(b) shows the single-line sintering at different line-scanning rates, where the laser power was 900 W and the scanning was 0.4–0.9 m/min. In the figure, the lines 1–6 are the single-line sintering pattern corresponding to the scanning rate 0.4–0.9 m/min, respectively. Line 1 appears coarse, which means it was not easy to control the precision of bulk formation. When the scanning rate was more than 0.7 m/min, it was not easy to sinter bulks due to disconnected sintering because

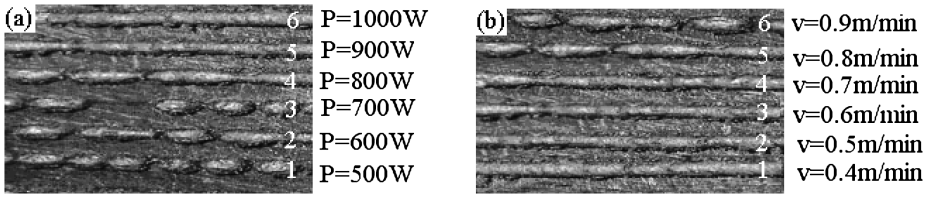

Figure 3. Photograph of single line laser sinter. (a) Different laser powers, (b) different scan rates.

the scanning rate was too high. The specimen of sintered bulk of a size 50 mm × 10 mm × 3 mm with the optimum process parameters (Table 1) is shown in Fig. 4.

4. Discussion

4.1. Microstructure Analysis

Figure 5 shows the microstructure of the laser sintered specimen, where the sintered organization is rather compact and there is no obvious laser sintered crack system and micro opening. It is concluded that the mixed powder enjoys good wetting and

Table 1.
The optimum process parameters

Process parameters	Optimum value
Spot diameter (mm)	1.0
Coating thickness (mm)	1.0
Scanning rate (m/min)	0.7
Laser power (W)	700
Scanning interval (mm)	1.0

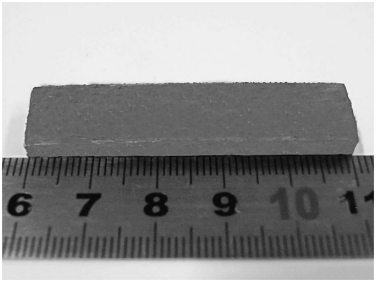

Figure 4. Photograph of laser sintered specimen.

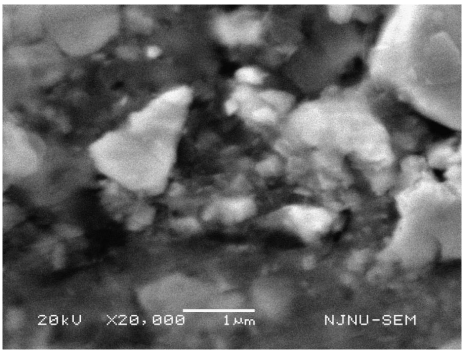

Figure 5. Cross-sectional microstructures of laser sintered specimen.

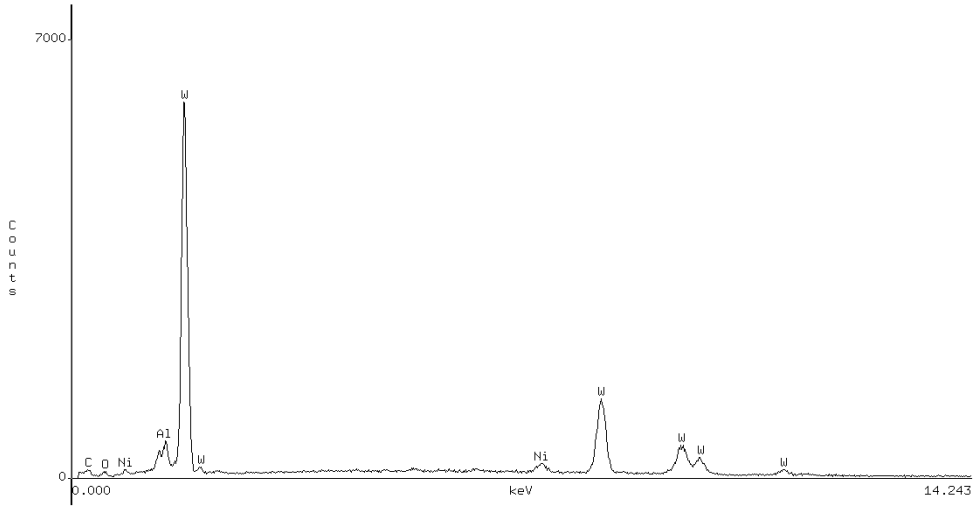

Figure 6. EDS spectrum of laser sintered specimen.

the reinforcement phase WC is dispersed in the matrix in the form of fine particles and dendritic crystals. The micro hardness on the cross-section of the specimen averages HV1183.6, which is markedly improved and rather uniform compared to the traditional high-temperature Ni-base alloy powder (HV486.7) [8]. This indicates that laser sintering was achieved evenly so that the mixed powder was bonded well.

The particle size of the irregular grey–white quadrangle is basically the same as the particle in the unsintered primitive compound powder, so this irregular quadrangle is the WC particle which still remains intact after sintering. In the compound powder, Ni has been completely fused during the sintering process and also has a very good inter-solubility with the WC particle, so the joining of the two interfaces is very close and without any interspace.

The marked irregular gray–white quadrangle was analyzed by EDS spectrum (Fig. 6). The result shows that the content of W has occupied absolute majority in this grey–white particle. In this particle, the content of W is 75.40 wt%. The content of Ni is 17.74 wt%. There is also 6.04 wt% C in this particle. Calculation gives us that these figures represent molar ratios of W at 31.10 mol and C at 38.16 mol. The proportion of these two elements is almost same as 1:1. In Fig. 2, the EDS spectrum of the primitive compound powder shows that there is still 7.43 mol carbon present, which represents a molar content that is almost the same as the exceeding part in Fig. 6. It shows that the grey–white particle is the WC micron particle in the primitive compound powder, which still remains intact after the sintering process with the laser that can heat and cool material at a high rate.

Figure 7 shows the X-ray diffraction pattern of the laser sintered specimen, where the diffraction peak of γ-Ni[Ni_3(Al, Ti) and WC is strong. Nickel base alloy powder can be melted and broken up by high-energy-density laser and compounded with Ti, Al to give a Ni_3(Al, Ti) metallic compound.

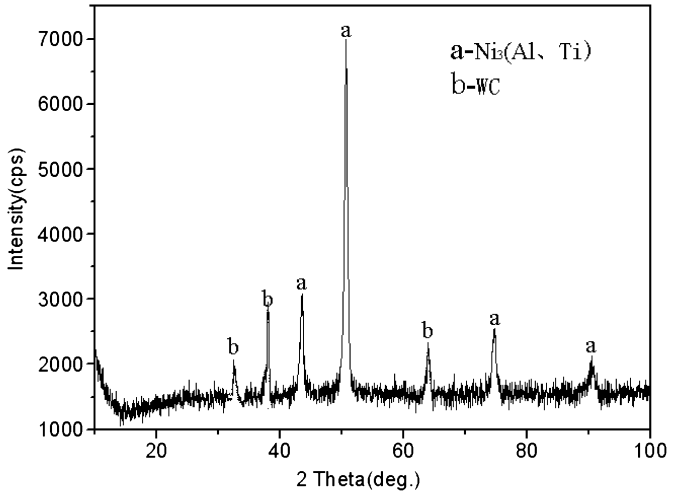

Figure 7. XRD pattern of laser sintered specimen.

It may be concluded that the phase of the sintered specimen mainly consists of γ-Ni and WC, both of which were not involved in chemical reaction, but the liquid phase sintering mechanism was realized soundly. In the course of sintering, Ni in the binding phase wrapping the surface of WC would be molten at the early stage of laser action and so would Ni-base powder, both with Ni as major element, enjoying good wettability and low thermal expansivity. While the sintering test was progressing, both of them wetted WC particles well; however, WC particles have an intrinsic fiber structure [9]. In the course of laser action, the largest energy absorbed by WC particles was not on the surface, but at a depth away from the surface [10, 11]. Therefore, under the action of high laser energy, the energy absorbed by WC particles was concentrated at a certain depth within them. The resulting impact causes fibrous-structured WC particles to be broken down into fine dendritic crystals. These, together with WC particles, lead to redistribution of the particles to change their position, and make them separate out by the force of the capillaries and the viscous flow of the liquid phase. Not only did the existence of dendritic crystals reinforce the phase of the matrix, but also served as transition between the WC particles and the matrix, so as to decrease laser thermal stress and micro crack.

4.2. Effect of Laser Power

Figure 8 shows the microstructure of a sintered specimen in different laser powers at a scanning rate 0.7 m/min with powder coated 0.20 mm thick. According to this figure, the density and uniformity of the sintered organization is obviously affected as the laser power changes.

At a low power of laser (800 W), serious agglomeration occurred with the WC particles; there were large pores between the reinforcement and the matrix, the sintered density was only 76.5% of the theoretical value (Fig. 8(a)), and the average micro hardness HV was only 918. With the laser power increasing to 900 W, WC

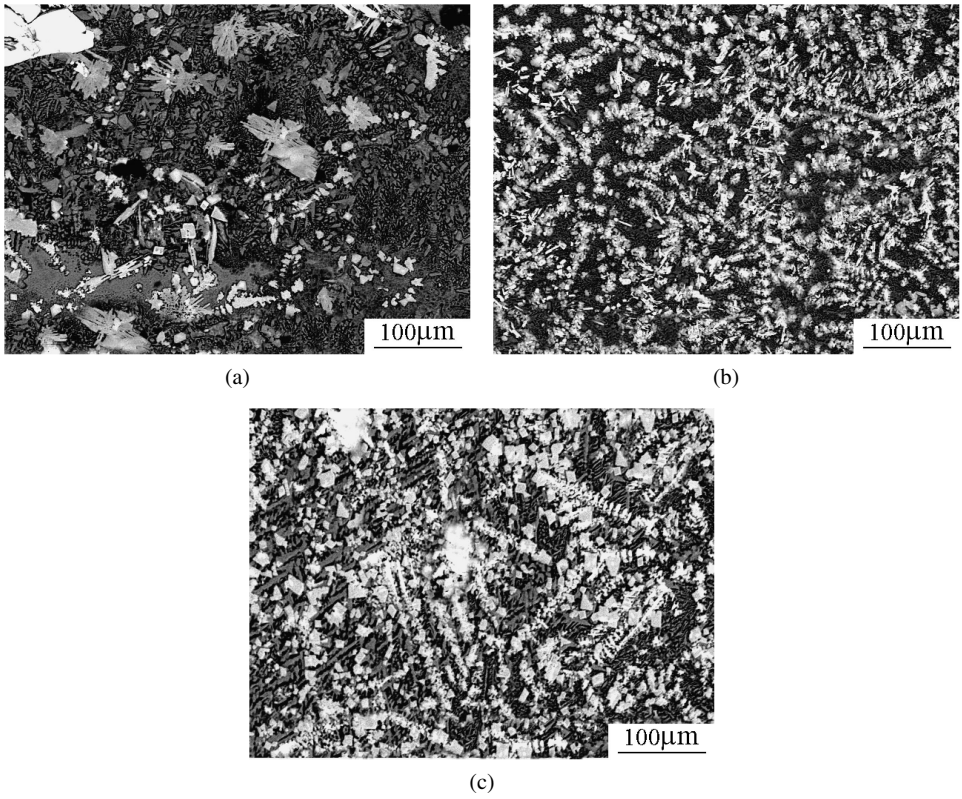

(a) (b)

(c)

Figure 8. Microstructures of surface of laser sintered specimens at different laser powers. (a) 800 W, (b) 900 W, (c) 1000 W.

particles were evenly distributed in the matrix in the form of dendritic crystals, well bonded to the matrix without pores in the interface; the sintered density increased rapidly, equal to 90.4% of the theoretical valve (Fig. 8(b)) and the average micro-hardness HV reached 1292. When the laser power reached 1000 W, the reinforced WC particles grew visibly large, although there were apparent pores in the sintered organization. The sintered density reduced to 82.6% of the theoretical value (Fig. 8(c)) and the average micro-hardness HV also decreased to 1003.

Sintering of both phases, solid and liquid, took place in the course of this reaction. Under the action of the laser, the liquid phase resulting from the matrix metal Ni was coated onto the surface of particles or gathered on the particle contact neck, so that WC particles were made to change their position and were redistributed by the force of the capillaries and the viscous flow of the liquid phase. Under the action of a low-power laser, the liquid phase resulting from the matrix metal Ni failed to wet WC particles sufficiently so that WC particles were not dissolved fully and the particles tended to agglomerate. Meanwhile, solid–liquid sintering occurred at the contact face of the particles, which caused apparent agglomeration between particles when separated out and produced apparent pores inside the sintered body.

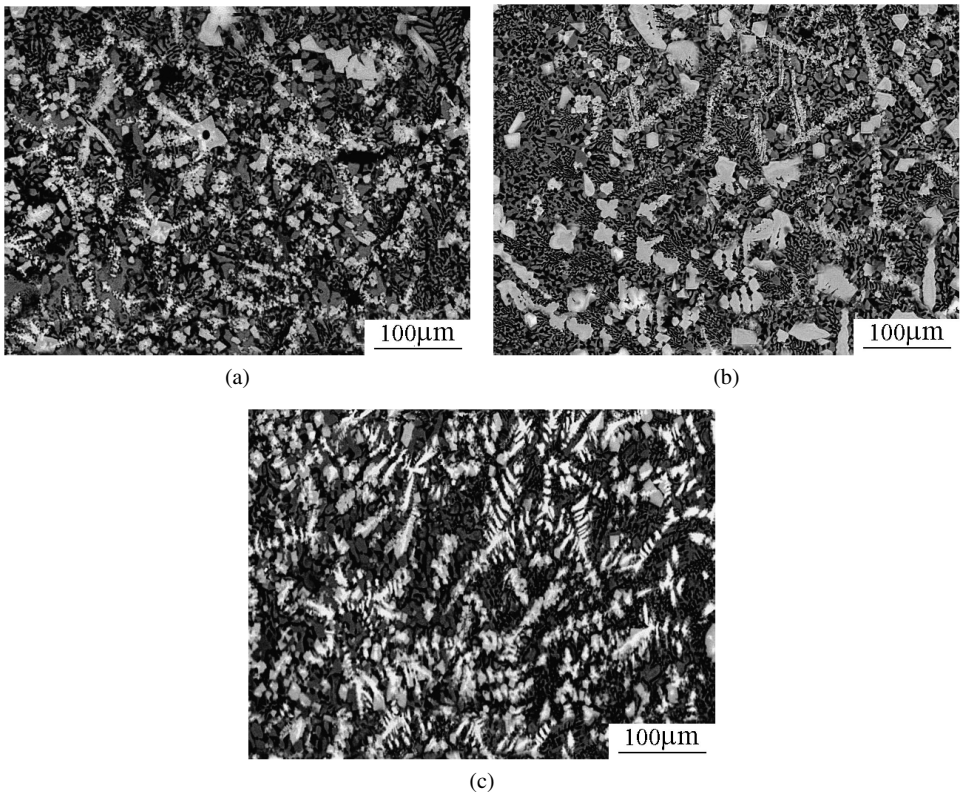

Figure 9. Microstructures of surface of laser sintered specimens at different scanning rates. (a) 0.5 m/s, (b) 0.6 m/s, (c) 0.7 m/s.

As the laser power was increased, the energy density increased, the sintered depth increased as particles were sintered fully, and the sintered density also increased. Meanwhile, the matrix metal liquid phase wetted WC particles fully, which, as a result, were rearranged by the force of the capillaries and the viscous flow of the liquid phase. Impacted by the high laser energy, WC particles were broken down to dendritic crystals so as to be distributed evenly in the matrix. However, a laser of too high a power (1000 W) would cause particles to be significantly gasified and the sintered density could not increase either. Additionally, WC particles, under high temperature, gathered together once more, grew large and produced layering, so that bulk formation was brought down and the control of its precision became difficult.

4.3. Effect of Scanning Rate

Figure 9 shows the microstructure of the laser sintered specimen at different scanning rates by employing a laser power of 900 W, with powder coated 0.20 mm thick. The scanning rate had a very noticeable effect on the uniformity of the reinforced particles distributed in the matrix. At a rather low rate (0.5 m/min), WC

particles were seriously agglomerated (Fig. 9(a)); when the scanning rate increased to 0.6 m/min, particle agglomeration still occurred locally (Fig. 9(b)); as the scanning rate went up continuously, the distribution uniformity of reinforced particles in the matrix improved significantly (Fig. 9(c)).

When the other parameters of laser remain invariable, the overall layout of WC particles in the matrix is dependent on the scanning rate. In the course of quick heating and setting by laser, the interface of the matrix will interact with particles. During liquid solidification, WC particles are either 'arrested' by the solid–liquid interface or pushed to form an aggregate as the solidification interface moves [12, 13]. The research indicates that when the solidification interface moved at a rate larger than a critical value, WC particles would be captured by the solid–liquid interface so that there was no agglomeration, and the moving rate of the interface solidification equaled the scanning rate of the laser [14, 15]. This critical scanning rate for optimal processing is approximately 0.7 m/min. When the laser scanning rate was larger than that, reinforced WC particles would be 'arrested' well by the solid–liquid interface and dispersed evenly in the matrix. However, if the scanning is too quick, there is too short a time left for the powder to be processed; this cannot ensure that the powder layer is sintered through, thus producing a defect in the layering, which may cause sintering to be discontinued. Therefore, this paper concludes that the optimal sintering rate is 0.7 m/min.

5. Conclusions

(1) The compound material of high-temperature Ni-base alloy bulks reinforced by WC particles was prepared by means of direct laser sintering. Some of the reinforced WC particles were molten and some decomposed. Alternatively, they were absolutely decomposed into fine dendritic crystals and separated out at the home position. Fully wetted by Ni base, the matrix and particles produced a very well bonded interface.

(2) When the laser power increased to 900 W, the laser sintering was the best in performance, the sintered density of bulks improved, and reinforced particles were evenly distributed in the matrix.

(3) When the scanning rate was larger than 0.7 m/min, the reinforced particles were arrested by the solid–liquid interface, so that WC particles were distributed well in the matrix, thus improving the performance of bulk sintering.

Acknowledgements

The work described in this paper was supported by the Science Foundation of Huaihai Institute of Technology (No. Z2009003), the Natural Science Foundation of China (No. 51004050), and the Huaihai Institute of Technology Introducing Talents Startup Foundation. Their contributions are gratefully acknowledged.

References

1. D. Gu and Y. Shen, Influence of reinforcement weight fraction on microstructure and properties of submicron WC–Cop/Cu bulk MMCs prepared by direct laser sintering, *J. Alloys Compounds* **2**, 112–120 (2007).
2. J. P. Kruth, G. Levy, F. Klocke and T. Childs, Consolidation phenomena in laser sintering and powder-bed based layer manufacturing, *Ann. CIRP* **56**, 730–759 (2007).
3. P. Yu and G. B. Schaffer, Microstructural evolution during pressureless infiltration of aluminium alloy parts fabricated by selective laser sintering, *Acta Mater.* **57**, 163–170 (2009).
4. S. Kumar and J.-P. Kruth, Composites by rapid prototyping technology, *Mater. Design* **31**, 850–856 (2010).
5. M. Zhong, W. Liu, Y. Zhang and X. Zhu, Formation of WC/Ni hard alloy coating by laser cladding of W/C/Ni pure element powder blend, *Intl J. Refract. Metals Hard Mater.* **24**, 453–460 (2006).
6. A. Simchi, Direct laser sintering of metal powders: mechanism, kinetics and microstructural features, *Mater. Sci. Engng: A* **428**, 148–158 (2006).
7. S. Rossi, F. Deflorian and F. Venturini, Improvement of surface finishing and corrosion resistance of prototypes produced by direct metal laser sintering, *J. Mater. Proc. Technol.* **148**, 301–309 (2004).
8. K. Maeda and T. H. C. Childs, Laser sintering (SLS) of hard metal powders for abrasion resistant coatings, *J. Mater. Proc. Technol.* **149**, 609–615 (2004).
9. J.-P. Kruth, G. Levy, F. Klocke and T. H. C. Childs, Consolidation phenomena in laser and powder-bed based layered manufacturing, *CIRP Annals — Manuf. Technol.* **56**, 730–759 (2007).
10. C. P. Paul and A. Khajepour, Automated laser fabrication of cemented carbide components, *Optics Laser Technol.* **40**, 735–741 (2007).
11. X.-B. Liu, G. Yu, J. Guo, Y.-J. Gu, M. Pang, C.-Y. Zheng and H.-H. Wang, Research on laser welding of cast Ni-based superalloy K418 turbo disk and alloy steel 42CrMo shaft, *J. Alloys Compounds* **453**, 371–378 (2008).
12. M. F. Chiang and C. Chen, Induction-assisted laser welding of IN-738 nickel-base superalloy, *Mater. Chem. Phys.* **114**, 415–419 (2009).
13. M. X. Li, Y. Z. He and G. X. Sun, Al_2O_3 nanocrystalline/Ni2 based alloy composite coatings produced by laser cladding, *Chinese J. Lasers* **31**, 1149–1152 (2004).
14. L. D. Shen, Y. H. Huang, Z. T. Tian and G. R. Hua, Direct fabrication of bulk nanostructured ceramic from nano-Al_2O_3 powders by selective laser sintering, *Key Engng Mater.* **329**, 613–618 (2007).
15. Z.-f. Xu, H. Yu, Y.-h. Zheng and C.-C. Cai, Preform of SiC ceramic particles by SLS and vacuum-pressure infiltration of aluminium, *Chinese J. Nonferr. Metals* **18**, 1864–1869 (2008).